Systems & Control Transactions

Research Article
Foundations of Computer Aided Process Design (FOCAPD 2024)
Breckenridge, Colorado, USA. July 14-18, 2024
Peer Reviewed Conference Proceeding

PSE PRESS

Membrane-based carbon capture process optimization using CFD modeling

Hector A. Pedrozo[a], Cheick Dosso[a], Lingxiang Zhu[b,c], Victor Kusuma[b,c], David Hopkinson[b], Lorenz T. Biegler[a], and Grigorios Panagakos[a,b,c,*]

[a] Dept. of Chem. Eng., Carnegie Mellon University, 5000 Forbes Ave, Pittsburgh, PA 15213, United States
[b] National Energy Technology Laboratory, 626 Cochran Mills Rd, Pittsburgh, PA, 15236, United States
[c] NETL Support Contractor, 626 Cochran Mills Rd, Pittsburgh, PA, 15236, United States
* Corresponding Author: gpanagak@andrew.cmu.edu

ABSTRACT

Carbon capture is a promising option to mitigate CO_2 emissions from existing coal-fired power plants, cement and steel industries, and petrochemical complexes. Among the available technologies, membrane-based carbon capture presents the lowest energy consumption, operating costs, and carbon footprint. In addition, membrane processes have important operational flexibility and response times. On the other hand, the major challenges to widespread application of this technology are related to reducing capital costs and improving membrane stability and durability. To upscale the technology into stacked flat sheet configurations, high-fidelity computational fluid dynamics (CFD) that describes the separation process accurately are required. High-fidelity simulations are effective in studying the complex transport phenomena in membrane systems. In addition, obtaining high CO_2 recovery percentages and product purity requires a multi-stage membrane process, where the optimal network configuration of the membrane modules must be studied in a systematic way. In order to address the design problem at process scale, we formulate a superstructure for the membrane-based carbon capture, including up to three separation stages. In the formulation of the optimization problem, we include reduced models, based on rigorous CFD simulations of the membrane modules. Numerical results indicate that the optimal design includes three membrane stages, and the capture cost is 45.4 \$/t-CO_2.

Keywords: Carbon Capture, Membranes, Computational Fluid Dynamics, Process Design, Optimization

INTRODUCTION

Climate change remains a relevant environmental concern with the global average temperature of Earth steadily rising, and this phenomenon is associated with the high concentration of carbon dioxide (CO_2) in the atmosphere. The current levels of carbon dioxide are over 50% greater than those observed prior to the industrial era, achieving values of 424 ppm of CO_2 concentration [1]. CO_2 takes the lead as the primary contributor to climate change, and human activities, especially CO_2 emissions from the energy and industrial sectors, are significant drivers.

In this context, carbon capture approaches offer hope in reducing greenhouse emissions since these processes can isolate carbon dioxide at point sources. Using this strategy, existing facilities can be retrofitted with capture plants, without changing the current industrial process significantly. Carbon capture technologies are crucial to achieving a net-zero emission scenario that limits the global average temperature increase below 1.5 °C [2]. Current CO_2 capture alternative pathways include absorption, adsorption, membrane-based, and cryogenic processes [3].

In contrast to adsorption and absorption, membrane-based carbon capture does not need a regeneration process, indicating potential capital and operating savings. Recent advancements in polymeric materials for gas separation, coupled with its straightforward plant design and operation, compactness, lightweight nature, and mobility, all combine to position membrane technology as a promising and feasible alternative for CO_2 capture [4].

Polymeric membranes present a range of advantages across diverse applications. Their straightforward fabrication simplifies technology adoption, ensuring accessibility and cost-effectiveness. Moreover, they exhibit reduced material requirements for module construction, offering both flexibility and cost savings. Additionally, their inherent processability empowers customization and adaptability, rendering them a versatile and appealing choice for various industries. For instance, the National Energy Technology Laboratory (NETL) has developed a rubbery thin film composite (TFC) membrane that exhibited high CO_2 permeance, high CO_2/N_2 selectivity, and stable performance in the presence of water vapor and non-aging behavior [5].

Several types of membrane modules are investigated in experimental work for flue gas separation [6]. Researchers frequently employ plate-and-frame (flat sheet), tubular, and hollow fiber membrane modules. In particular, the plate-and-frame configuration offers the benefit of a low-pressure drop, which holds greater significance in high-volume, low-pressure applications. In addition, this kind of membrane is easy to clean and to replace. On the other hand, additional supports are required for the membrane, and it offers low area-to-volume ratios.

When compared to modeling approaches, conducting CFD simulations can be a cost-effective and efficient means to simultaneously study variable effects while ensuring accuracy in the outputs [7]. Specifically, CFD techniques provide the capability to analyze polymeric membranes under conditions that surpass the limits of experiments, enabling the generation of diverse trend analyses for better comprehension of the model results. CFD analysis proves valuable for assessing the viability and performance of specific membrane modules for industrial applications.

Regarding the implementation of the technology at process scale, it was concluded that a single-stage membrane process is unable to achieve high capture rates and high purity simultaneously [8,9]. Therefore, multi-stage membrane processes have been proposed to overcome this issue. In order to address the design problem using a holistic approach, membrane systems engineering has evolved as an important research area to understand the trade-offs among operating variables at plant scale, through mathematical modeling, simulations, and optimization techniques. In this context, superstructure optimization plays a crucial role in the formulation of the optimization problems since it involves creating a comprehensive network that includes all possible components, units, and interconnections relevant to the case study. Qi and Henson [10] addressed the separation of acid gases (CO_2 and H_2S) from crude natural gas, by introducing a superstructure with potential network configurations obtained through a strategic arrangement of mixers, splitters, and compressors. Arias et al. [11] used mathematical programming and superstructure-based optimization to design multi-stage CO_2 capture membrane systems, to find the optimal configuration of membrane stages, areas, power requirements, recycle stream placement, and operational conditions.

In this work, we formulate a superstructure optimization for the optimal design of a membrane-based carbon capture process, where we use rigorous CFD simulations to build the models for the membrane modules.

METHODOLOGY

Based on the literature [10,11], we formulate the superstructure shown in Fig. 1 for the optimal design of the multi-stage membrane process for carbon capture. In the present work, we demonstrate the potential of the technology using three separation stages. However, based on the application and the end goals, we could increase the number of stages as needed.

The input stream can be conditioned by increasing its pressure and/or a cooling operation. Then, the input stream could be sent to any of three possible membrane stages. For each membrane stage, the input stream, the retentate product, and the permeate product stream could be pressurized if this operation contributes to increasing the objective function. In addition, the permeate product could be cooled if required. It should be noted that this superstructure configuration embeds the potential process configurations, and the membrane order is not fixed beforehand. On the contrary, the order is determined based on the configuration that optimizes the objective function of the problem.

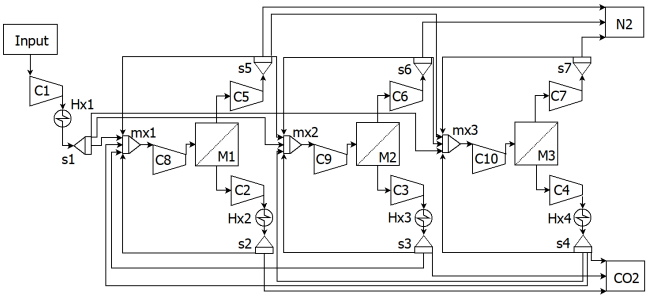

Figure 1. Superstructure for the optimal design of the multi-stage membrane process for carbon capture. M: membrane separation stage. C: compressor. Hx: heat exchangers. s: splitters. mx: mixers.

In order to model the superstructure of Fig. 1, we develop mathematical models for each equipment unit, and we consider the connections between them. Our modeling framework is mainly based on the literature[12,13] for the general process units, including the compressors, the heat exchangers, the mixers, and the splitters. For the calculation of the compound properties,

we fit polynomials based on the data from Aspen Plus, and we consider ideal gas thermodynamics calculations.

The objective function is the minimization of the capture cost, and it is defined as follows

$$CapCost = \frac{(\phi+\varpi)\cdot CAPEX + OPEX + M_{REP}}{F_{CO_2}} \quad (1)$$

where $CAPEX$ and $OPEX$ are the capital and operating costs, respectively; ϕ is the capital recovery factor (0.154), ϖ is a factor to consider the annual maintenance cost (0.045), M_{REP} is the annualized replacement cost of the membrane modules, and F_{CO_2} is the flowrate of the captured CO_2 in the plant. The $CAPEX$ is calculated from the purchased equipment cost of individual equipment units, and we use the cost correlations reported in [14], while the capital costs are updated to 2023 dollars by using a Chemical Engineering Plant Cost Index (CEPCI) of 803.3.

Regarding the membrane modules, we formulate a model including mass and enthalpy balances for the membrane modules, and we consider the operation of them in parallel. To calculate the CO_2 recovery and the purity product in the permeate we also develop surrogate models based on a rigorous CFD model, which is described in the next section.

Rigorous CFD simulation

The representation of the CFD model for the membrane module is shown in Fig. 2. We consider a 3D geometry that includes two main parts: the retentate side and the permeate side. The input CO_2-rich stream enters the feed side, and carbon dioxide efficiently crosses through the selective boundary to the permeate side, where a concentrated CO_2 stream is recovered. This technology utilizes thin film composite membranes consisting of rubbery polymer blends [5], without the inclusion of carriers.

We implement the CFD model in Comsol Multiphysics to describe the separation process using membranes. For this, we use the Navier-Stokes equation to calculate the velocity distribution, considering compressible laminar flow with Mach number less than 0.3, as shown in Eq. (2):

$$(\boldsymbol{u}\cdot\boldsymbol{\nabla})\boldsymbol{u} - \nu\nabla^2\boldsymbol{u} + \frac{1}{\rho}\nabla p = 0 \quad (2)$$

where $\boldsymbol{u}$ is the velocity, p is the pressure, ν is the kinematic viscosity and ρ is the density.

Regarding the mass transfer phenomena, we use the physics for transport of concentrated species, by considering the following expression:

$$\rho\boldsymbol{u}\cdot\nabla\omega_i + \boldsymbol{\nabla}\cdot\left(-\rho(D_i\boldsymbol{\nabla}\omega_i)\right) = 0 \quad (3)$$

where ω_i is the mass fraction of species i, and D_i is the diffusion coefficient of species i.

For both retentate and permeate sides, we consider the coupled phenomena, which include the physics of the laminar flow and the mass transport. However, these domains have different reference pressures since the retentate side operates near atmospheric pressure and the permeate side usually operates under vacuum. The driving force for the species flow through the selective boundary is the CO_2 partial pressure difference; increasing this pressure difference increases the stage cut of the membrane process.

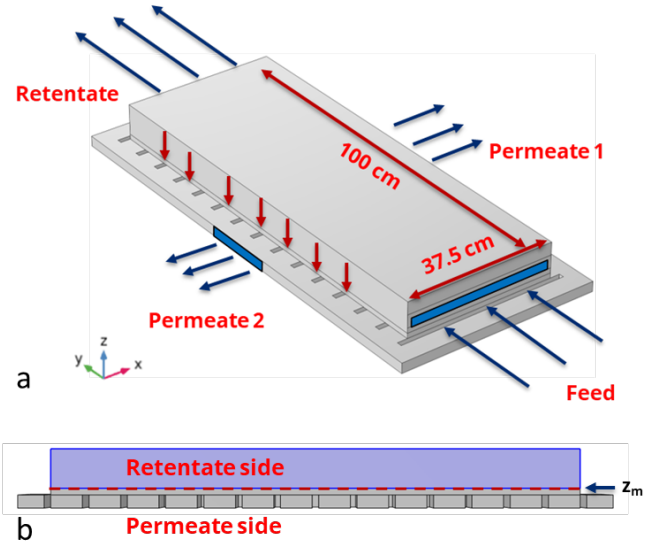

Figure 2. CFD model for the membrane module. a) Main configuration and flux directions. b) Domains and selective boundary

In order to model the membrane separation process, we define the selective boundary layer as a boundary condition for both physics. This selective layer is located at a height z_m in the membrane module, as shown in Fig. 2. The species fluxes ($J_{x,i}, J_{y,i}, J_{z,i}$) are given by Eq. (3) in the transport phenomena, considering experimental data for the permeance of CO_2 and N_2 as pure gases (Q_i). In this way, the modeling approach considers the different mass transfer resistances due to the membrane. Therefore, we do not have to include the information associated with the porosity of the support in the model. Regarding the velocity profile calculation, we consider a leaking wall as a boundary condition, calculating the equivalent velocity to satisfy momentum balances (see Eq. (4)).

$$z = z_m \rightarrow \begin{cases} J_{x,i} = 0 \\ J_{y,i} = 0 \\ |J_{z,i}| = Q_i M_i (p^{ret} x_i^{ret} - p^{per} x_i^{per}) \end{cases} \quad (3)$$

$$z = z_m \rightarrow \begin{cases} u_x = 0 \\ u_y = 0 \\ u_z = -\frac{1}{\rho}\sum_{i\in\{CO_2,N_2\}} J_{z,i} \end{cases} \quad (4)$$

where Q_i is the permeance of species i, and M_i is the molar mass of species i.

Regarding the boundary conditions for the inlet and outlet streams, we use the conventional approach to specify them, as explained in [15]. In particular, we run the CFD model several times to generate data for the reduced model generation, as we explain below. In this matter, we consider inlet mass flowrates between 40-220 mg/s, inlet CO_2 concentrations between 0.1 and 0.7, retentate outlet pressures between 1.02-2 atm, and permeate outlet pressures between 0.09-0.6 atm.

Model simplification and mesh studies

To enhance the computational tractability of the CFD model, a symmetry plane has been introduced for the membrane module. This modification involves the incorporation of a yz plane, resulting in a halved geometry, as depicted in Fig. 3. In this way, the number of cells required for the mesh is also halved.

Regarding the mesh, we have developed a mapped mesh for the geometry as shown in Fig. 3. This meshing technique has shown a superior performance for mesh generation, offering the possibility of reducing the required number of cells to achieve accurate results.

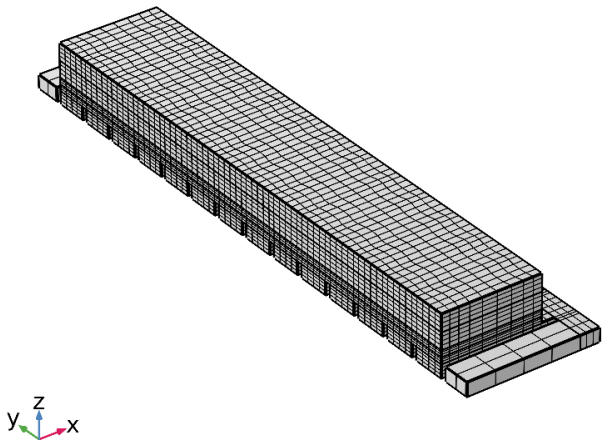

Figure 3. Mesh for the membrane module (637,460 degrees of freedom)

For the present case study, we perform a mesh independence study to select an appropriate number of mesh elements. This analysis is shown in Fig. 4, where we show the influence of degrees of freedom, directly proportional to the number of mesh nodes, on the CO_2 recovery of the membrane module for the mapped mesh and the free tetrahedral mesh. The results indicate that as the mesh becomes finer, the CO_2 recovery decreases for the free tetrahedral mesh and increases for the mapped mesh. In addition, it is observed that the number of degrees of freedom to obtain accurate results is lower for the mapped mesh. It is worth noting that beyond 637,460 degrees of freedom, there is no significant change in the CO_2 recovery. The relative difference between this point and the one with the highest number of nodes (which is also the most accurate) is only 0.076%. This suggests that a mesh containing 637,460 degrees of freedom provides sufficient computational accuracy.

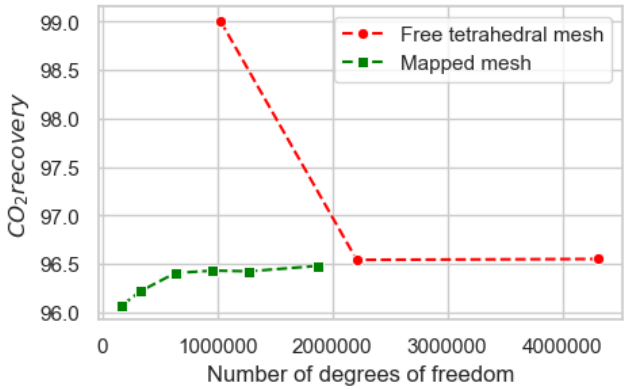

Figure 4. Variation of the CO_2 recovery with the degrees of freedom in the mesh. Input flow: 1250 SCCM; x_{CO_2}:0.3; p^{ret}: 1.2 bar; p^{per}: 0.2 bar.

Surrogate model for the membrane process

The CFD for the membrane module was validated using experimental data, as described in the literature [16], for a bench-scale experimental implementation. In the present work, we have scaled up the membrane module to a length of 1 m and a width of 0.375, as shown in Fig .2. Then, from this model, we generate sampling data and build a reduced model by using kriging-based methodology available in the IDAES computational framework [17]. This modeling approach considers a correlation function between different sampling points, which is usually called kernel. In the present case, we use the Gaussian kernel ($k(\boldsymbol{x}_i, \boldsymbol{x}_j)$), which is shown in Eq. (5).

$$k(\boldsymbol{x}^i, \boldsymbol{x}^j) = exp\left(-\sum_{r=1}^{d} \theta_r \left|x_r^i - x_r^j\right|^2\right) \quad (5)$$

where $\boldsymbol{x}^i$ and $\boldsymbol{x}^j$ are sampling points, $\boldsymbol{\theta} = \{\theta_1, \theta_2, \ldots, \theta_d\}^T$ is vector associated with the length scale hyperparameters, and d is the dimension of the input variable vector. The values of output variables are calculated through the following expression:

$$y_* = \mu + \boldsymbol{k}_*^T(\boldsymbol{K} + \sigma^2 \boldsymbol{I_n})^{-1}(\boldsymbol{y} - \boldsymbol{1}\mu) \quad (6)$$

where y_* is the expected value of the output variable, μ is the mean, n is the number of sample points, $\boldsymbol{I_n}$ is the identity matrix of dimension n, σ is the regularization parameter associated with the noise of the data and $\boldsymbol{y}$ is the vector of the sampled output variable. The vector $\boldsymbol{k}_*$ and the matrix $\boldsymbol{K}$ are calculated through Eqs. (7) and (8), considering the Gaussian correlation function (see Eq. (5)).

$$[\boldsymbol{K}]_{i,j} = k(\boldsymbol{x}^i, \boldsymbol{x}^j) \quad (7)$$

$$[\boldsymbol{k}_*]_i = k(\boldsymbol{x}^i, \boldsymbol{x}^*) \quad (8)$$

In particular, we build reduced models that consider the

following input variables: i) inlet flowrate; ii) pressure in the retentate; iii) pressure in the permeate; iv) inlet CO_2 concentration. On the other hand, we consider the CO_2 recovery and the CO_2 purity in the permeate side as output variables for the model. In this way, we can exploit the information of the rigorous CFD simulation to create a reduced model, which is implemented in the superstructure for the selection of the multistage membrane process.

Table 1. Main statistics metrics of the Kriging model for the CO_2 recovery (output variable)

CO_2 recovery	Training data	Validation data
R^2	1.0000	0.9992
Mean squared error	$2.6 \cdot 10^{-6}$	$4.7 \cdot 10^{-5}$
Mean rel. error (%)	0.2819	1.5116
Max. rel. error (%)	2.1905	5.9386

The main performance metrics for our built-reduced models are shown in Table 1. It is observed that the performance of the built reduced models is appropriate for their implementation in the optimization model since the R^2 coefficients are close to one, for both output variables. In addition, the statistics metrics for the training and the validation data do not change significantly, indicating a low risk of overfitting.

Table 2. Main statistics metrics of the Kriging model for the CO_2 purity in the retentate (output variable)

Purity	Training data	Validation data
R^2	1.0000	0.9998
Mean squared error	$4.8 \cdot 10^{-7}$	$8.0 \cdot 10^{-6}$
Mean rel. error (%)	0.1266	0.4301
Max. rel. error (%)	0.7907	1.9357

RESULTS

In the present work, we consider the optimal design of a plant to treat a flue gas of 30 % CO_2 -70% N_2 and a molar flow rate of 1000 mol/s, as a case study. This CO_2 concentration is representative of steel plants but our model can account for any set of inlet and operating conditions. We set the lower bounds for CO_2 recovery and the purity at 80 % and 90 %, respectively.

The mathematical programming model is implemented in Pyomo and solved using IPOPT [18]. As commercial solvers for global optimization turn out to be inefficient in solving the present problem design, we use a multi-start approach to increase the possibility of finding the global optimal solution.

The optimization problem includes 539 variables and 50 optimization variables. We note that the use of reduced models reduced the problem complexity significantly since the rigorous simulation of each membrane separation stage includes 637,460 variables. Therefore, solving the full optimization model for optimal design represents computational challenges, which would be the bottleneck of any decision-making. It is only through surrogate models that we can seek a practical design optimization in an acceptable timeline.

The main economic indicators are shown in Table 3. The objective function is the capture cost, for which we obtain a value of 45.4 \$/t-CO_2. This value is of the expected order for a multi-stage membrane process [6]. The total annual cost for the capture plant is also shown in Table 1. The main contributor to this economic indicator is the annualized capital cost (51 %), while the operating cost represents 29 % of the total annual cost. Our results indicate that the capital cost associated with compressors accounts for 65 % of the CAPEX, while the membrane cost is 33%. It should be noted that the purity and the CO_2 recovery are at their lower bounds for the optimization problem.

Table 3. Economic indicators associated with the optimal design of the membrane-based carbon capture

	Value
Capture cost (\$/t-CO_2)	45.69
Total annual cost (MM\$/y)	13.89
Capital cost (MM\$)	46.25
Operating cost (MM\$/y)	4.00
Purity (%)	90
CO_2 recovery (%)	80

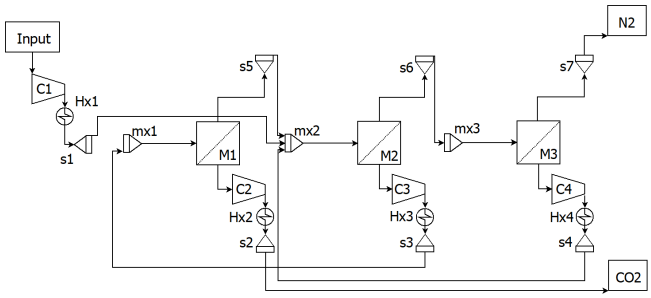

Figure 5. Optimal configuration for the membrane process. M: membrane separation stage. C: compressor. Hx: heat exchangers. s: splitters. mx: mixers.

The optimal configuration for the membrane-based carbon capture process is shown in Fig. 5. It comprises a three-stage membrane separation setup. The inlet flue gas is introduced into the second membrane module, M2. The retentate product from M2 is fed to the third module, M3, where a N_2-rich stream is recovered in the retentate stream, while the permeate side is recirculated back to M2. The permeate stream originating from M2 is then

sent to the first module, M1, which yields the purified CO_2 stream. The retentate product from M1 is also recycled to M2 for further processing.

It should be noted that the optimal network for the separation process using membranes is not trivial, and there is a trade-off between the recovery and purity in each separation stage. At process level, there are also trade-offs related to recycled streams; high recirculation rates increase the operating costs but they have the potential to reduce the required membrane area. In this context, the proposed superstructure optimization is a valuable tool for finding a solution, considering these process interactions in the design.

Regarding the operating condition and separation performance of the membrane stages, Table 4 shows the main results. It is observed that the membrane M2 includes a higher area than M1 and M3, and this result is associated with its high inlet flow (recycling streams for M1 and M3 are sent to M2 in the process network). In addition, we observe that M1 operates at high inlet CO_2 concentration to achieve the target purity of the CO_2 product (90 %), while M3 operates with a CO_2-dilute stream (15 %) to recover the greenhouse gas before expelling the N_2-rich stream from the retentate of this membrane stage. The permeate side for the membrane stages is at vacuum pressure, while the retentate is at atmospheric pressure. M2 and M3 operate at low pressure (0.1 atm) in the permeate side to promote CO_2 transport through the selective layer; while the pressure of the permeate side of M1 is 0.4 atm. For each membrane stage, we also report the dimensionless feed flow and the retentate recovery, which are associated with the capital cost and the energy requirement [19], respectively.

In order to verify the accuracy of the reduced models in the environment of the optimal solution, we have run the rigorous CFD simulation considering the input variables reported in Table 4 for each membrane stage. These input variables include the inlet flow, the inlet CO_2 molar fraction, and the pressure of the retentate and the permeate sides. The results associated with this analysis are shown in Table 5. In general, we obtained relative differences between the reduced model and the rigorous CFD simulations lower than 1 %. The sole exception is the prediction of the reduced model for the CO_2 purity for M3, which is 5 % lower than the value obtained by the CFD simulation. This means that the objective function of the optimization problem could slightly improve by updating the reduced model with this information. Future work will focus on using the trust-region filter method [20,21] to solve the problem and obtain highly accurate solutions

Table 4. Operating conditions and results for the membrane stages

	M1	M2	M3
Membrane area (m^2)	30,849	107,800	54,887
Inlet flow (mol/s)	565	1465	901
Inlet CO_2 molar fraction	0.70	0.36	0.15
Retentate pressure (atm)	1.02	1.02	1.02
Permeate pressure (atm)	0.40	0.11	0.10
CO_2 recovery	0.61	0.74	0.55
CO_2 purity	0.90	0.70	0.42
Dimensionless feed flow	0.33	0.25	0.30
Retentate recovery	0.53	0.62	0.81

Table 5. Output variables from the rigorous CFD simulations and the NLP model (calculated from the Kriging approach), using the input variables shown in Table 4

	M1	M2	M3
CO_2 recovery (CFD model)	0.608	0.740	0.551
CO_2 recovery (NLP model)	0.614	0.745	0.552
CO_2 purity (CFD model)	0.906	0.701	0.445
CO_2 purity (NLP model)	0.900	0.700	0.423

The CO_2 molar fraction profile (x_{CO_2}) of membrane stage M2 is shown in Fig. 6. Initially, the inlet x_{CO_2} is 0.36, while the retentate outlet x_{CO_2} is 0.15. The decrease in x_{CO_2} is attributed to the selective CO_2 flow through the membrane selective layer during the separation process. In the permeate region close to the feed, x_{CO_2} reaches high purities of up to 0.90. However, as we move closer to the permeate side near the retentate outlet, the CO_2 purity decreases to around 0.50. Consequently, the average CO_2 purity of the outlet permeate flow is estimated to be approximately 0.70.

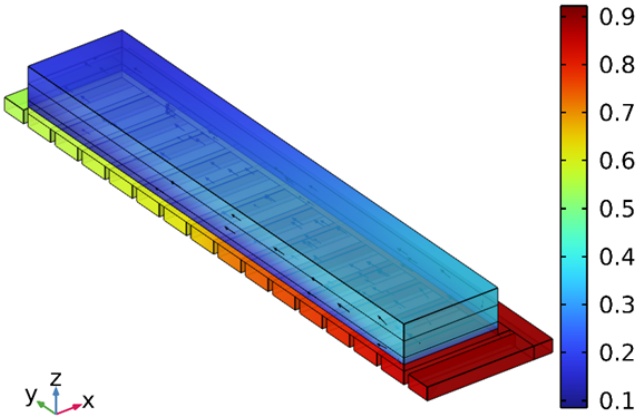

Figure 6. Profile of CO_2 molar fraction (x_{CO_2}) for M2. Input flow: 86.06 mg/s; x_{CO_2}:0.36; p^{ret}: 1.02 atm; p^{per}: 0.11 atm.

Effect of the CO_2 concentration in the feed stream

We also explore the effects of changing the CO_2 molar fraction in the feed stream on key parameters, such as the objective function (capture cost), the membrane area, and the energy demand. For this purpose, we run the optimal design problem by considering different inlet CO_2 molar fractions in the interval of 0.2-0.3, while keeping the input molar flowrate of CO_2 constant.

The results associated with this analysis are shown in Table 6. In all of the cases, the purity and the CO_2 recovery were found at their lower bounds, 90 % and 80 %, respectively. It is observed that the capture cost decreases significantly as the inlet CO_2 molar fraction increases. These results are in agreement with the literature [14]. This trend can be explained by the simultaneous reduction in both membrane area and energy demand as the inlet CO_2 molar fraction rises, as detailed in Table 6.

Table 6. Effect of the inlet CO_2 concentration of the feed in the capture cost, membrane area, and energy demand

Inlet CO_2 molar fraction	Capture cost ($/t-$CO_2$)	Membrane area (m2)	Energy demand (kWh/t-CO_2)
0.2	73.13	371,880	284.5
0.225	64.77	320,059	252
0.25	57.90	277,819	231.4
0.275	52.01	244,103	206.51
0.3	45.69	193,536	182.8

CONCLUSIONS AND FUTURE WORK

In this work, we address the optimal design of a multi-stage membrane process for carbon capture. For this task, we develop a CFD model of a membrane module, from which we generate a Kriging reduced model to be implemented in an optimization problem. In order to design the separation network, we formulate a superstructure to consider a three-stage membrane process. As the main case study, we consider an inlet flue gas stream with a CO_2 molar fraction of 30 % and a molar flowrate of 1000 mol/s. However, our computational framework is flexible and versatile and can therefore be adapted to accommodate various inlet and operating conditions to simulate any post-combustion or industrial plant and real-life gas stream compositions. Our work could also be extended to inform both new plants and to retrofit existing ones.

Our results show that the optimal design includes the three membrane stages and the capture cost of the process is 45.69 $/t-$CO_2$. Determining the resulting network configuration and optimal operating conditions for the membrane stages is a non-trivial task. In this context, the optimization formulation shows its value as it determines optimal trade-offs between the decision variables.

Future work will focus on including additional design variables associated with the membrane module, i.e., geometric variables. In addition, we will include the effect of temperature on the transport phenomena for the CFD model. Regarding the solution strategy, we will solve the problem by using trust region methods, to guarantee the optimality of the solution.

ACKNOWLEDGEMENTS

This project was funded by the United States Department of Energy, National Energy Technology Laboratory, in part, through a site support contract. Neither the United States Government nor any agency thereof, nor any of their employees, nor the support contractor, nor any of their employees, makes any warranty, express or implied, or assumes any legal liability or responsibility for the accuracy, completeness, or usefulness of any information, apparatus, product, or process disclosed, or represents that its use would not infringe privately owned rights. Reference herein to any specific commercial product, process, or service by trade name, trademark, manufacturer, or otherwise does not necessarily constitute or imply its endorsement, recommendation, or favoring by the United States Government or any agency thereof. The views and opinions of authors expressed herein do not necessarily state or reflect those of the United States Government or any agency thereof.

REFERENCES

1. National Oceanic and Atmospheric Administration. Broken record: Atmospheric carbon dioxide levels jump again. (2023)
2. Shu DY, Deutz S, Winter BA, Baumgärtner N,

Leenders L, Bardow A. The role of carbon capture and storage to achieve net-zero energy systems: Trade-offs between economics and the environment. *Renew Sustain Energy Rev*. 178:113246 (2023)
3. Kazemifar F. A review of technologies for carbon capture, sequestration, and utilization: Cost, capacity, and technology readiness. *Greenh Gases Sci Technol* . 12(1):200–30 (2022)
4. Pasichnyk M, Stanovsky P, Polezhaev P, Zach B, Šyc M, Bobák M, Jansen JC, Přibyl M, Bara JE, Friess K, Havlica J. Membrane technology for challenging separations: Removal of CO_2, SO_2 and NO_x from flue and waste gases. *Sep Purif Technol*. 323:124436 (2023)
5. Zhu L, Kusuma V, Hopkinson D. Highly Permeable Thin-Film Composite Membranes of Rubbery Polymer Blends for CO_2 Capture. In United States; (2022).
6. Chatziasteriou CC, Kikkinides ES, Georgiadis MC. Recent advances on the modeling and optimization of CO_2 capture processes. *Comput Chem Eng*. 165:107938 (2022)
7. Sithamparam M, Lai LS, Tay WH. Computational fluid dynamics simulation for carbon dioxide gas transport through polydimethylsiloxane membrane with gyroid structure. *Mater Today Proc*. 46:1922–1928 (2021)
8. Khalilpour R, Abbas A, Lai Z, Pinnau I. Modeling and parametric analysis of hollow fiber membrane system for carbon capture from multicomponent flue gas. *AIChE J* . 58(5):1550–61 (2012)
9. Brunetti A, Scura F, Barbieri G, Drioli E. Membrane technologies for CO_2 separation. *J Memb Sci*. 359(1):115–25 (2010)
10. Qi R, Henson MA. Optimal design of spiral-wound membrane networks for gas separations. *J Memb Sci* .148(1):71–89 (1998)
11. Arias AM, Mussati MC, Mores PL, Scenna NJ, Caballero JA, Mussati SF. Optimization of multi-stage membrane systems for CO_2 capture from flue gas. *Int J Greenh Gas Control*. 53:371–90 (2016)
12. Pedrozo HA, Rodriguez Reartes SB, Vecchietti AR, Diaz MS, Grossmann IE. Optimal Design Of Ethylene And Propylene Coproduction Plants With Generalized Disjunctive Programming And State Equipment Network Models. *Comput Chem Eng*. 149:107295 (2021)
13. Dowling AW, Biegler LT. A framework for efficient large scale equation-oriented flowsheet optimization. *Comput Chem Eng*. 72:3–20 (2015)
14. Hasan MMF, Baliban RC, Elia JA, Floudas CA. Modeling, Simulation, and Optimization of Postcombustion CO_2 Capture for Variable Feed Concentration and Flow Rate. 1. Chemical Absorption and Membrane Processes. *Ind Eng Chem Res*. 51(48):15642–64 (2012)
15. Comsol Multiphysics®. User's Guide. Version 6.2 (2023).
16. Dosso C, Zhu L, Kusuma VA, Hopkinson D, Biegler LT, Panagakos G. CFD Modeling of High-Flux Plate-and-Frame Membrane Modules for Post-Combustion Carbon Capture. In: AIChE Annual Meeting. Orlando, FL; (2023)
17. Lee A, Ghouse JH, Eslick JC, Laird CD, Siirola JD, Zamarripa MA, Gunter D, Shinn JH, Dowling AW, Bhattacharyya D, and Biegler LT. The IDAES process modeling framework and model library—Flexibility for process simulation and optimization. J Adv Manuf Process. 3(3):e10095 (2021)
18. Wächter A, Biegler LT. On the implementation of an interior-point filter line-search algorithm for large-scale nonlinear programming. *Math Program*. 106(1):25–57 (2006)
19. Sun L, Panagakos G, Lipscomb G. Effect of Packing Nonuniformity at the Fiber Bundle-Case Interface on Performance of Hollow Fiber Membrane Gas Separation Modules. *Membranes* 12(11):1139 (2022)
20. Eason JP, Biegler LT. Advanced trust region optimization strategies for glass box/black box models. *AIChE J*. 64(11):3934–3943 (2018)
21. Pedrozo HA, Panagakos G, Biegler LT. Including CFD rigorous models in the optimal design of carbon capture plants through trust-region methods. *Chemical Engineering Science*. 286, 119646 (2024)